Thermohaline forcing of eastern boundary currents: With application to the circulation off the west coast of Australia

by Julian P. McCreary, Jr.,[1] Satish R. Shetye[2] and Pijush K. Kundu[1]

ABSTRACT

The linear, viscid, continuously stratified model of McCreary (1981) is extended to allow for thermohaline forcing by a specified, longitudinally independent, surface density field ρ_s. When the ocean is unbounded and ρ_s is steady, the density field is altered throughout the water column by vertical diffusion. If ρ_s increases poleward, the resulting pressure field slopes downward toward the pole in the upper water column, and there is an associated eastward geostrophic current. This interior current forces downwelling at an eastern ocean boundary, and generates a poleward surface coastal current and an equatorward undercurrent. For realistic choices of model parameters the coastal circulation is as strong as, and opposite in direction to, that caused by a typical equatorward wind stress τ^y. When ρ_s oscillates at the annual cycle, the unbounded flow is confined to a surface boundary layer. The coastal circulation is qualitatively quasi-steady, but also has characteristics of a vertically propagating Kelvin wave.

One solution is forced by an idealized representation of the observed ρ_s and τ^y fields off the west coast of Australia. This solution compares well with observations of the oceanic circulation there. In particular, there is a surface coastal jet (the model Leeuwin Current) that flows against the wind. This successful comparison suggests that the mean circulation in the region is significantly forced by ρ_s, whereas the annual variability is strongly forced by τ^y.

1. Introduction

The prevailing winds along subtropical eastern ocean boundaries generally have an equatorward component. Such winds drive an offshore surface drift and force upwelling at the coast. As a result, the near-surface isopycnals slope upward and the surface dynamic height field decreases toward the coast, and there is a narrow geostrophically balanced alongshore surface current that flows in the direction of the wind. Coastal sea level slopes downward toward the pole, so that the surface current flows against a pressure gradient. At depths of about 100–300 m there is a poleward coastal undercurrent.

The coastal circulation off the west coast of Australia is strikingly different, even though the wind is directed equatorward throughout the year (Thompson, 1984;

1. Nova University, Oceanographic Center, 8000 N. Ocean Drive, Dania, Florida, 33004, U.S.A.
2. National Institute of Oceanography, Dona Paula, Goa 403 004, India.

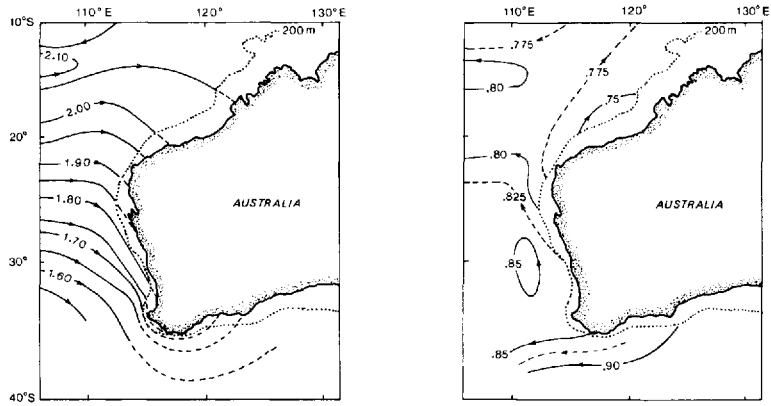

Figure 1. Annual average dynamic height relative to 1300 db at sea level (left panel) and at 450 db (right panel). The dotted line shows the position of the 200 m isobath. Sea level offshore drops 35 cm from 22S to 32S, indicating a geostrophic flow of the order of 7 cm/s toward Australia. Sea level also drops toward the coast in the same latitude band, suggesting the presence of a narrow, southward, coastal current. Dynamic height at 450 db is much flatter, but does indicate the existence of a northward undercurrent. There is a dome of dynamic height marked .85db located just off the coast. (After Godfrey and Ridgway, 1985.)

Godfrey and Ridgway, 1985). There is little evidence of coastal upwelling, and near-surface isopycnals slope *downward* toward the coast. There is a narrow *poleward* surface current (the recently discovered Leeuwin Current) and an *equatorward* undercurrent (Figs. 1 and 2). Despite the opposing wind the Leeuwin Current intensifies as it flows poleward, attaining an annual mean speed greater than 50 cm/s near Perth (Godfrey, private communication). As in other regions, coastal sea level slopes downward toward the pole (Fig. 1); thus, the surface current flows *with* the coastal pressure gradient. Finally, the Leeuwin Current attains its maximum strength in the southern-hemisphere winter when the alongshore winds are weakest (see the discussion of Fig. 10).

These observations all indicate that some mechanism other than offshore Ekman drift drives the coastal flow field off Australia. One possible mechanism is local forcing by wind curl. The local wind curl, however, is almost always positive (Godfrey and Ridgway, 1985), and so favors the development of an equatorward, rather than poleward, surface current. A second possibility is remote forcing by some process located equatorward of the observations. Godfrey and Ridgway (1985), for example, have suggested that the Leeuwin Current may be remotely forced by the high surface dynamic height field that appears near the Australian coast north of 20S in the southern-hemisphere winter. [The cause of this dynamic height field is not clear. One intriguing hypothesis suggested by Godfrey (private communication) is that it is associated with the flow of low-density Pacific Ocean water into the Indian Ocean through the Indonesian Archipelago.] Remote forcing, however, is not likely to be the

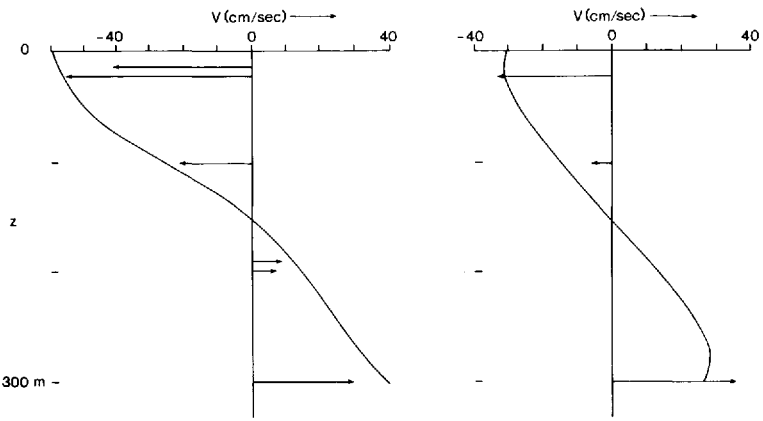

Figure 2. Observed equatorward velocity component of the currents off the west coast of Australia at 25.4S (left panel) and at 22S (right panel). The arrows are measurements from a current meter; the curve from geostrophy using 150 m as a level of no motion. The undercurrent is nearly as strong as the surface flow. The Leeuwin Current strengthens to the south. (After Thompson, 1984).

dominant mechanism driving the current; a remotely forced coastal current should weaken away from the forcing region, contrary to the observed intensification apparent in Figures 1 and 2.

A third possibility is thermohaline forcing due to the poleward increase of surface density in the ocean interior (Shetye, 1984; Thompson, 1984). At mid-latitudes this increase is due primarily to the poleward cooling of the sea surface, typically 10–20°C per 20° of latitude (Charts II and III of Sverdrup *et al.*, 1942); in the southern Indian Ocean there is an additional salinity gradient that intensifies the increase (Chart VI of Sverdrup *et al.*, 1942). A consequence of this density change is that the dynamic height of the sea surface drops toward the poles. In the southern Indian Ocean the drop is 40 cm from 20S to 30S (Fig. 96c of Stommel, 1965; Fig. 1 here). Such a sea-surface tilt is associated with a geostrophic eastward surface current of the order of 10 cm/s, potentially a significant source of water for driving an eastern boundary current at the Australian coast.

In this paper we extend the coastal model of McCreary (1981) to include thermohaline forcing in the form of a specified surface density field ρ_s. Our approach is similar to that used by Rothstein (1984), who forced an equatorial model with a specified ρ_s. The model is three-dimensional, linear, continuously stratified and viscid. A simplifying assumption is that the alongshore current is geostrophically balanced, a restriction that allows solutions to be represented in a simple analytic form. Solutions are found for both steady and periodic forcings.

Important results are the following. As expected, when ρ_s increases poleward an eastward geostropic current is established in the interior ocean. At an eastern ocean boundary this interior flow forces coastal downwelling, a poleward surface current and

an equatorward undercurrent. For realistic choices of model parameters this coastal circulation is comparable in magnitude, but opposite in direction, to that driven by an equatorward wind τ^y. The circulation off Australia is simulated by forcing the model with a steady ρ_s and a seasonally varying τ^y, and the model response compares well with several observed features.

2. The ocean model

a. Equations and boundary conditions. The equations of motion, linearized about a state of no motion with density $\rho_b(z)$ and Väisälä frequency $N_b(z)$, are

$$\begin{aligned} -fv + p_x &= 0, \\ v_t + fu + p_y &= G + (\nu v_z)_z + \nu_h v_{xx}, \\ u_x + v_y + w_z &= 0, \\ \rho_t - N_b^2 w/g &= (\kappa\rho)_{zz} + \kappa_h \rho_{xx}, \\ p_z &= -\rho g, \end{aligned} \tag{1}$$

where the coefficients of vertical eddy viscosity and diffusivity have the form

$$\nu = \kappa = A/N_b^2. \tag{2}$$

Coefficients of horizontal eddy viscosity and diffusivity are ν_h and κ_h, respectively, and we assume that $\nu_h = \kappa_h$. The coordinates (x, y, z) and the velocity components (u, v, w) are directed eastward, northward and upward, respectively; the coast is oriented along the y-axis, and the origin is placed at the surface-coast corner. The pressure and density changes from the background state are p and ρ. The Coriolis parameter is $f = 2\Omega\sin(y/R)$, where $\Omega = 2\pi$ day^{-1} and R is the radius of the earth. The parameter g is the acceleration due to gravity. The meridional wind stress is assumed to enter the ocean as a body force, $G = \tau^y/h$, spread uniformly over a surface layer of thickness h. Constant factors of the average background density are everywhere ignored.

Eqs. (1) involve several assumptions that are essential to the method of solution used here (McCreary, 1981). First, the vertical diffusion of density is expressed as $(\kappa\rho)_{zz}$ instead of the usual $(\kappa\rho_z)_z$, and the vertical mixing coefficients are inversely proportional to N_b^2. Only by adopting these forms for vertical mixing is it possible to represent solutions as expansions in the vertical normal modes of the system. Second, the alongshore velocity field is taken to be in geostrophic balance. Third, the operator ∇^2 in the horizontal diffusion terms is replaced by ∂_{xx}. The last two restrictions allow solutions to be expressed in a simple analytic form.

It would be better if both ν and κ were related to the Richardson number of the flow, as is done in some numerical models (see, for example, Pacanowski and Philander,

1981). The effect of this parameterization is to allow for large values of ν and κ in the coastal ocean where the current shear is strong, and for small values in the interior ocean. Such mixing coefficients cannot be used in the present linear analytic model, but it is possible to simulate their effect by allowing A to have different values for different parts of the solution. As we shall see, the solution is expressed as the sum of a forced interior solution and a coastal response, and we regard each piece to be associated with its own value of A.

Surface boundary conditions are

$$\nu v_z = w = 0, \rho = \rho_s \qquad \text{at } z = 0. \tag{3}$$

The no-stress condition is sensible, because the effect of forcing by the wind is assumed to be taken up entirely by the body force G. Bottom boundary conditions are

$$\nu v_z = w = \kappa\rho = 0 \qquad \text{at } z = -D, \tag{4}$$

where D is the depth of the ocean.

Solutions to (1), subject to conditions (3) and (4), can be expressed in terms of the vertical eigenfunctions $\psi_n(z)$ as

$$(u, v, p) = \sum_{n=1}^{N} (u_n, v_n, p_n)\psi_n, \qquad w = \sum_{n=1}^{N} w_n \int_{-D}^{z} \psi_n dz, \qquad \rho = \sum_{n=1}^{N} \rho_n \psi_{nz}, \tag{5}$$

where the eigenfunctions satisfy the equation

$$\psi_{nz} = -\frac{N_b^2}{c_n^2} \int_{-D}^{z} \psi_n dz, \tag{6}$$

subject to the constraint

$$\frac{1}{c_n^2} \int_{D}^{0} \psi_n dz = 0, \tag{7}$$

and they are normalized so that $\psi_n(0) = 1$. The barotropic mode ($n = 0$) makes a negligible contribution to the solution, and so is neglected throughout. The $n \geq 1$ modes form an infinite set of baroclinic modes. The summation over the baroclinic modes is necessarily truncated at a finite value N.

The expansion coefficients, functions only of x, y and t, are given by

$$\begin{aligned} -fv_n + p_{nx} &= 0, \\ (\partial_t + A/c_n^2)v_n + fu_n + p_{ny} &= G_n + \nu_h v_{nxx}, \\ (\partial_t + A/c_n^2)p_n + c_n^2(u_{nx} + v_{ny}) &= Q_n + \kappa_h p_{nxx}, \\ w_n &= (\partial_t + A/c_n^2 - \kappa_h \partial_{xx})p_n/c_n^2 - Q_n/c_n^2, \\ \rho_n &= -p_n/g, \end{aligned} \tag{8}$$

and the coupling coefficients of each mode to the surface forcing are

$$Q_n = -\frac{g\kappa_s\rho_s}{\int_{-D}^{0}\psi_n^2\,dz}, \qquad G_n = \frac{(\tau^y/h)\int_{-h}^{0}\psi_n dz}{\int_{-D}^{0}\psi_n^2\,dz}, \tag{9}$$

where κ_s is the value of diffusivity at the ocean surface. A set of equations similar to (8), including the density forcing term Q_n, was derived by Rothstein (1984). McCreary (1981) introduced wind stress into the ocean in a surface mixed layer where $N_b = 0$; such a mixed layer cannot be included here, since in that case $\kappa_s = A/N_b^2 = \infty$ and Q_n is not well defined.

Eqs. (8) are solved either in an unbounded basin or in a semi-infinite basin with an eastern boundary. No-slip conditions are imposed if there is an eastern boundary, so that

$$u_n = v_n = 0 \qquad \text{at } x = 0. \tag{10}$$

In addition, the solutions must remain finite in the far field as $x \longrightarrow -\infty$.

b. The solution. We now find solutions to (8) when the imposed forcings are periodic with a frequency σ and have the forms

$$\rho_s = \rho_0\, Y_1(y)e^{-i\sigma t}, \qquad \tau^y = \tau_0\, Y_2(y)e^{-i\sigma t}. \tag{11}$$

The meridional profiles Y_1 and Y_2 are arbitrary functions, except that Y_{1y} and Y_2 must be zero near the equator where solutions are not valid [as is apparent in solution (13), for example]. For mathematical convenience, both ρ_s and τ^y are taken to be independent of x, although it is possible to extend the formalism to allow for x-dependent forcings (as in McCreary and Kundu, 1985).

An equation for p_n alone, derived from the first three of Eqs. (8), is

$$\nu_h p_{nxxxx} + i\omega p_{nxx} - \kappa_h\alpha^2 p_{nxx} - \beta p_{nx} - i\omega\alpha^2 p_n = \alpha^2 Q_n, \tag{12}$$

where $i\omega = i\sigma - A/c_n^2$, $\alpha^{-1} = c_n/f$ is the Rossby radius, and $\beta = f_y$. The method of solution is essentially to solve (12) for p_n, and then to use (8) to represent u_n, v_n, w_n and ρ_n in terms of p_n. Solutions are conveniently written as the sum of an unbounded response (primed variables) and a boundary contribution (double-primed variables) that ensures that the coastal boundary conditions (10) are satisfied.

i. The unbounded response. Since Q_n and G_n are independent of x, so is the unbounded (forced) solution of (12). The resulting flow field is

$$\begin{aligned} p_n' &= -\,Q_n/i\omega, \\ u_n' &= Q_{ny}/i\omega f + G_n/f, \\ v_n' &= w_n' = 0, \\ \rho_n' &= Q_n/i\omega g. \end{aligned} \tag{13}$$

(Note that the above set becomes invalid at the equator where $u'_n = \infty$, a consequence of the assumption of alongshore geostrophy.) Two terms contribute to the zonal velocity field. The contribution G_n/f is the Ekman drift associated with each baroclinic mode (McCreary, 1981). The other contribution $Q_{ny}/(i\omega f)$ represents a geostrophic, eastward, surface current when there is a poleward increase of surface density.

The interior pressure and velocity fields are determined from (13) by summing over all vertical modes as in (5). The summation for the density field, however, is not uniformly convergent. It does not converge to the correct density at the ocean surface, since $\psi_{nz} = 0$ there. To avoid this mathematical difficulty we determine ρ' directly by solving the density equation in (1) with $w' = \rho'_{xx} = 0$,

$$-i\sigma\rho' = (\kappa\rho')_{zz} = A(\rho'/N_b^2)_{zz}, \tag{14}$$

subject to $\rho' = \rho_s$ at $z = 0$. The steady ($\sigma = 0$) solution of (14) is $\rho' = \rho_s(1 + z/D)N_b^2(z)/N_b^2(0)$. For the general periodic case, (14) is solved by finite differencing over 5000 points in the vertical.

It is interesting that the steady solution (13) is *independent* of the strength of vertical mixing in the model, since both Q_n and ω are proportional to A. [Note also that the steady state solution to (14) is independent of A.] The thermodynamic reason for this property is that in the steady state even a vanishingly small amount of vertical diffusion is sufficient to diffuse density throughout the water column. This property is nice, since it is then possible to regard this solution as being associated with the small values of κ that are generally thought to be applicable in the interior ocean ($\kappa \sim .1 - 1$ cm^2/s).

ii. The boundary contribution. Contributions to the solution due to the presence of the eastern boundary are free solutions of (12) and (8). It follows that

$$\begin{aligned}
p''_n &= \sum_{j=1}^{2} P_j e^{ik_j x}, \\
u''_n &= \frac{1}{f^2}\sum_{j=1}^{2} (-\omega k_j - i\nu_h k_j^3 - f\partial_y) P_j e^{ik_j x}, \\
v''_n &= \frac{i}{f}\sum_{j=1}^{2} k_j P_j e^{ik_j x}, \\
w''_n &= \frac{1}{c_n^2}\sum_{j=1}^{2} (-i\omega + \kappa_h k_j^2) P_j e^{ik_j x}, \\
\rho''_n &= -p''_n/g,
\end{aligned} \tag{15}$$

where $P_1(y)$ and $P_2(y)$ are amplitude functions, and k_1 and k_2 are the two roots of

$$\nu_h k^4 + (-i\omega + \kappa_h\alpha^2)k^2 - i\beta k - i\omega\alpha^2 = 0 \tag{16}$$

that have negative imaginary parts. The boundary conditions (10) require that $u'_n + u''_n = 0$ and $v'_n + v''_n = 0$ at $x = 0$, yielding two equations for P_1 and P_2. Their solution is

easily shown to be

$$P_1 = \frac{k_2 e^{-\Lambda}}{k_2 - k_1} \int_{y_0}^{y} e^{\Lambda} f u_n' dy, \qquad P_2 = -\frac{k_1}{k_2} P_1, \tag{17}$$

where

$$\Lambda = -\int^{y} \frac{i\nu_h}{f} k_1 k_2 (k_1 + k_2) dy \tag{18}$$

(McCreary, 1981). The lower limit y_0 of the y-integration in (17) is any point equatorward of the forcing, whereas the lower limit of the integral in (18) is arbitrary.

c. Rossby and Kelvin waves. What sort of waves contribute to the solution (15)? To answer this question it is convenient first to consider the waves that exist in the inviscid model. Modifications due to mixing are briefly discussed at the end of this subsection.

Without mixing the dispersion relation (16) reduces to the quadratic equation

$$\sigma k^2 + \beta k + \sigma \alpha^2 = 0, \tag{19}$$

which has the single eastern-boundary root

$$k_1 = -\frac{\beta}{2\sigma}\left[1 - \left(1 - 4\frac{\sigma^2\alpha^2}{\beta^2}\right)^{1/2}\right]. \tag{20}$$

Since $\alpha = 0$ at the equator and $\beta = 0$ at the poles, the radicand in (20) vanishes at some intermediate latitude, the critical latitude, being given by

$$\theta_{cr} = \tan^{-1}(c_n/2R\sigma). \tag{21}$$

The nature of the boundary waves changes markedly depending on whether θ is greater or less than θ_{cr}. Poleward of θ_{cr}, k_1 is complex and (20) represents β-plane Kelvin waves that decay offshore rapidly with an e-folding scale of the order of α^{-1}; equatorward of θ_{cr}, k_1 is real and the waves are Rossby waves that propagate, rather than decay, offshore (Moore, 1968; McCreary, 1980).

The value of θ_{cr}, and hence the type of waves that contribute to (15), depends on both σ and modenumber n. In the low-frequency, quasi-steady limit where $\sigma \ll c_n/2R$, θ_{cr} approaches $\pi/2$ and the boundary waves associated with many baroclinic modes are Rossby waves. Conversely, in the high-frequency limit where $\sigma > c_1/2R$, θ_{cr} tends to zero and the boundary waves are all Kelvin waves. At the annual cycle θ_{cr} typically occurs outside the tropics for only a few low-order baroclinic modes. For example, for the background density field used here (Fig. 3) the critical latitudes for the first three baroclinic modes are 46N, 29N and 20N, respectively. Poleward of 20N, then, most of the boundary waves are Kelvin waves; only the $n = 1$ and 2 waves are Rossby waves.

The presence of horizontal mixing in the model does not significantly modify the

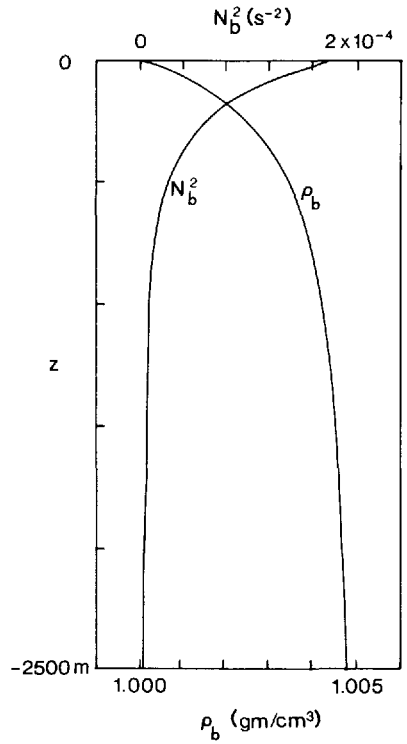

Figure 3. Profiles of the assumed background density ρ_b and the square of its Väisälä frequency N_b^2. The structure of ρ_b is defined precisely in (23).

waves; the Rossby waves are hardly changed at all because their zonal wavelengths are large, and the offshore structure of the Kelvin waves is altered so as to bring v to zero at the coast. When there is weak vertical mixing, as is true for the low-order baroclinic modes in the model, the viscid waves still have properties similar to those discussed above. They differ in that they are now damped in the direction of their group velocity and the critical latitude is not so sharply defined. When vertical mixing is strong, there is no longer a clear distinction between Rossby and Kelvin waves.

3. Results

a. Choice of parameters The solutions in this paper are driven by density forcing alone, except that the solution in section 3d is forced by a combination of surface density and wind. They are all calculated in the northern hemisphere, but symmetry ensures that they are also applicable in the southern hemisphere. We adopt a sea-surface temperature change of 15°C per 20° of latitude, corresponding to a surface density change $\rho_0 = 3.3 \times 10^{-3}$ gm/cm^3, and assume a linear increase of the surface

density from 20N to 40N. Thus, ρ_s is given by

$$\rho_s = \begin{cases} -\rho_0 e^{-i\sigma t}, & y \le 20\text{N} \\ -\rho_0 \left(\dfrac{40° - y}{20°}\right) e^{-i\sigma t}, & 20\text{N} \le y \le 40\text{N} \\ 0, & y \ge 40\text{N}. \end{cases} \tag{22}$$

The value of σ is either 0 or 2π year^{-1}.

Figure 3 shows the background density profile chosen. It is given by the double-exponential profile.

$$\rho_b = 1 + \Delta\rho_1(1 - e^{z/b_1}) + \Delta\rho_2(1 - e^{z/b_2}), \tag{23}$$

where $\Delta\rho_1 = .003$ gm/cm^3, $b_1 = 200$ m, $\Delta\rho_2 = .002$ gm/cm^3, and $b_2 = 1000$ m. This profile has a strong near-surface pycnocline. It is necessary to adopt such a profile in order to minimize density inversions that develop near the ocean surface when ρ_s is sufficiently large (see the discussion in section 3b). The depth of the ocean is 2500 m.

Unless specified otherwise, the horizontal mixing coefficients are $\nu_h = \kappa_h = 10^5$cm^2/s. The vertical mixing coefficients vary considerably with depth according to (2), with a minimum value $\nu_{\min}$ occurring at the surface where the Väisälä frequency is maximum. Unless specified otherwise, $\nu_{\min}$ for the coastal contribution (15) is 10 cm^2/s (so that $A = 1.7 \times 10^{-3}$cm^2/s^3). With this choice the values of ν in the deep coastal ocean are unrealistically large; as noted below, however, the most significant effect of this increase is to weaken the model coastal undercurrent at depth. The steady interior solution (13), which is independent of $\nu_{\min}$, is assumed to be associated with a small value of heat diffusion; the periodic interior solution in Figure 9 has $\nu_{\min} = 10$ cm^2/s. Effects of varying both ν_h and $\nu_{\min}$ are reported at several points in the text.

The upper limit N in the sum (5) is always 100. This number is sufficient to ensure that solutions have converged.

b. Steady density-driven flow. In this subsection we discuss solutions forced by the steady ($\sigma = 0$) surface density field (22). Figure 4 shows the unbounded response, and Figures 5–7 illustrate the circulation when there is an eastern boundary.

Figure 4 shows a meridional section across the x-independent unbounded solution (13). Sea level at the southern edge is 68 cm higher than it is at the northern edge, and this slope drives a geostrophic eastward flow in the upper ocean. The flow weakens poleward because of the increase of f. Both the pressure gradient and the associated zonal flow reverse direction in the deep ocean. The perturbation density ρ' is linear in y, and has a sharp vertical gradient near the surface. It is this interior flow field that drives the coastal circulation in Figures 5–7.

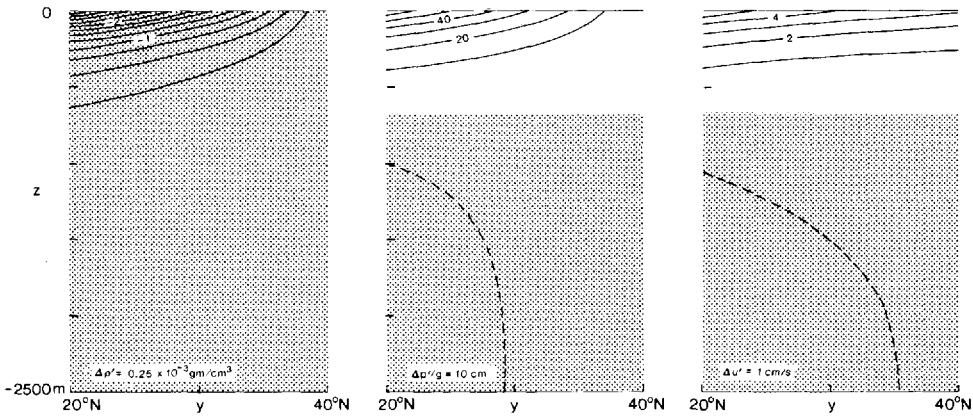

Figure 4. A meridional section showing the model response in an unbounded ocean to a steady surface density forcing of the form (22). The figure shows ρ', p' and u' in the left, center and right panels, respectively. Negative regions are shaded. Dashed contours are midway between the indicated contour interval. The poleward increase in ρ' causes a decrease in p' and an eastward geostrophic current u' near the ocean surface. The zonal current u' extends much deeper into the water column than a comparable one forced by the wind. It is this interior current that drives the coastal circulation in Figures 5–7.

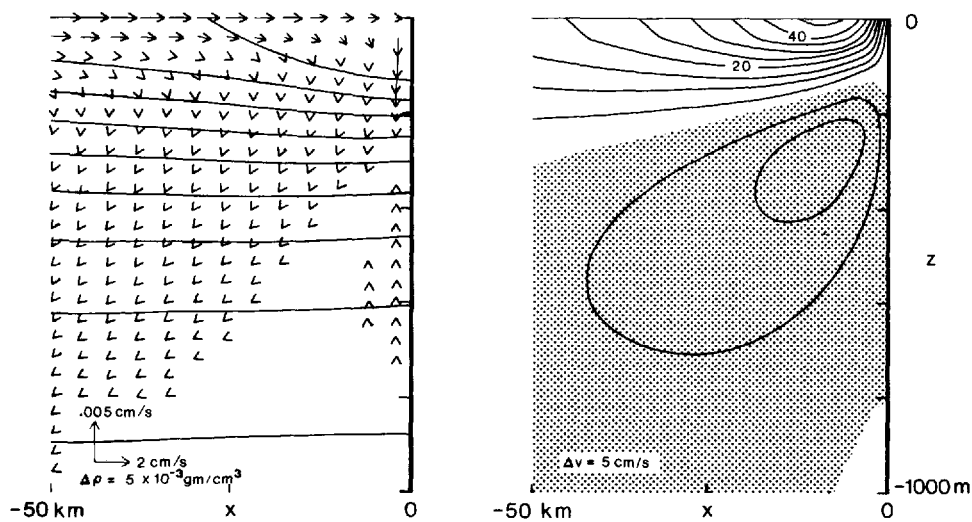

Figure 5. A zonal section at 40N showing u, w and ρ in the left panel and v in the right panel when the forcing is a steady ρ_x. Regions of negative (equatorward) flow are shaded. There is coastal downwelling to a depth somewhat greater than 200 m, and near-surface isopycnals bend down toward the coast. There is a strong poleward surface current and a weaker equatorward undercurrent.

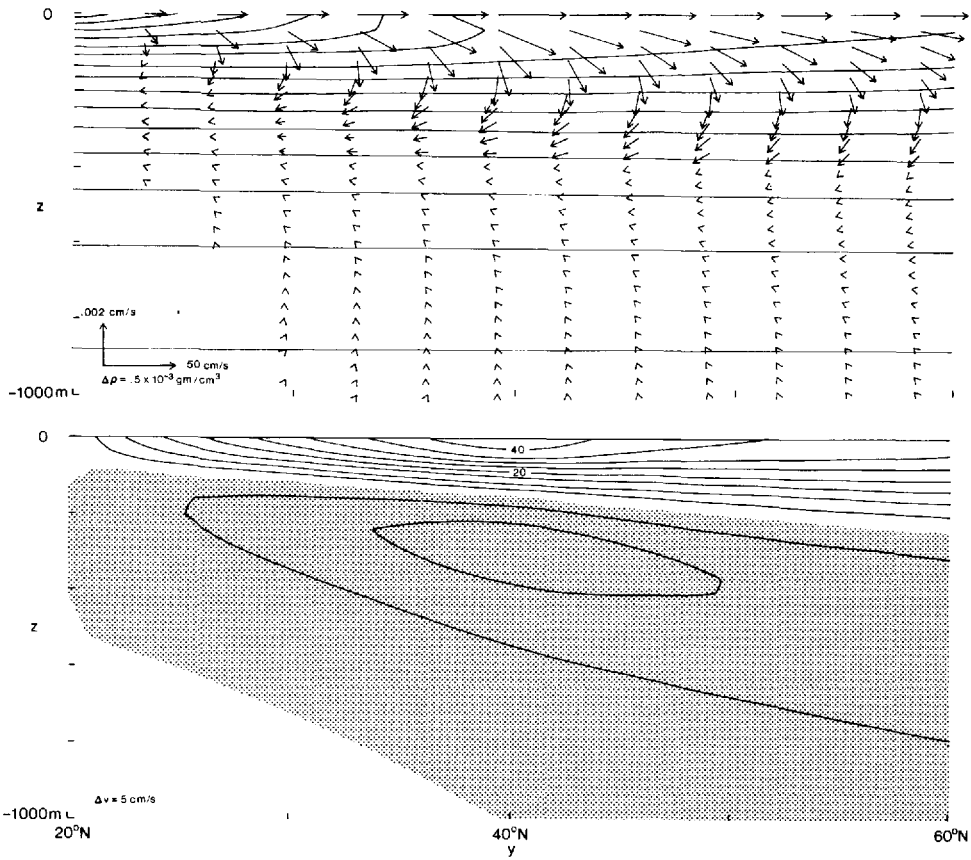

Figure 6. A meridional section showing v, w and ρ in the upper panel and contours of v in the lower panel when the forcing is a steady ρ_s. The section is located at $x = -8$ km, the distance offshore at which the alongshore currents achieve their maximum speeds (Fig. 5). Regions of negative (equatorward) flow are shaded. The alongshore currents increase in strength to 40N, the northern edge of the forcing region. There is a weak density inversion at the ocean surface from about 35N to 40N.

The vertical structure of the zonal current in Figure 4 is very different from that of the analogous wind-driven flow, which is contained entirely in the thin surface mixed layer. The reason for this difference is that in steady state the effect of ρ_s on the density field is not confined to a surface boundary layer; according to (14), the forcing is felt throughout the water column. The difference in boundary-layer structure is also apparent from a comparison of the two terms in (13) that contribute to u_n', namely $Q_{ny}/(i\omega f) = c_n^2 Q_{ny}/(Af)$ and G_n/f. Because c_n decreases roughly like n^{-1}, low-order modes make a relatively larger contribution to the density-driven currents, which therefore extend deeper into the water column.

Figure 5 shows a zonal section at the northern edge of the forcing, $y = 40$N, when

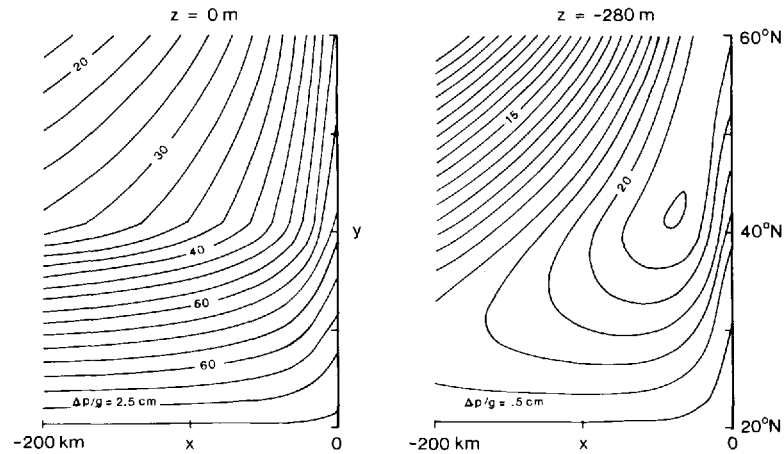

Figure 7. Horizontal sections showing the pressure field in dynamic centimeters at the sea surface (left panel) and at a depth of 280 m (right panel) when the forcing is a steady ρ_s. Sea level 200 km offshore drops 40 cm from 20N to 40N and also rises toward the coast. At 280 m depth the pressure field is much flatter, and the coastal pressure increases toward the pole. Compare this figure to the observations off Australia in Figure 1.

there is an eastern boundary. The surface current is poleward and has a maximum speed of 47 cm/s, and there is an equatorward undercurrent with a maximum speed of 13 cm/s at a depth of 280 m. The zonal flow in the upper ocean is onshore with a speed of 1.6 cm/s at $x = -50$ km, whereas the deeper flow is offshore. There is coastal downwelling near the surface, with w attaining a minimum value of -3.6×10^{-3} cm/s $= -3$ m/day, and weak upwelling below the undercurrent core. In accordance with alongshore geostrophy, density surfaces slope downward in the upper ocean and slightly upward at depth.

Figure 6 shows a meridional section of the flow at $x = -8$ km, the offshore distance at which the alongshore currents are strongest (Fig. 5). The speeds of the alongshore currents increase poleward, reaching maximum values at the northern edge of the forcing region. Physically, the reason for this increase is that the coastal currents are driven by the interior flow that is present throughout the forcing region (Fig. 4); the surface current must strengthen to provide an outlet for this onshore flow. Mathematically, the increase occurs because the amplitudes of the boundary solution (17) involve a poleward integration.

There is a region of density inversion evident in Figures 5 and 6, located near the coast-surface corner in a latitude band from 35N–40N. The inversion is the result of the linearization of the vertical advection term in the density equation of (1). Because N_b is not allowed to vary with time in this equation, downwelling always causes density to decrease, and when w_z is sufficiently large and positive an inversion can occur. (With a nonlinear density equation, where N_b is allowed to change, a well-mixed upper layer near the coast would be obtained instead of a density inversion.) The amplitude of the

inversion is small, and can be eliminated completely if the strength of the forcing is decreased somewhat or ρ_b is allowed to have a sharper surface pycnocline.

Figure 7 shows the horizontal structure of the perturbation pressure field at the surface (left panel) and at the depth of the undercurrent core (right panel). The model pressure distributions are strikingly similar to the observed dynamic height distributions of Figure 1. At the offshore edge ($x = -200$ km) the model sea surface falls by 37 cm between 20N and 40N. Sea level falls at a slower rate farther north and at the coast. The subsurface pressure field has a dome around which there is anticyclonic flow; it may not be a coincidence that a similar dome is also present in the observed dynamic height field. Note that both the surface current and the undercurrent flow in the direction of the coastal pressure gradient. This property differs from wind-driven coastal circulation where the surface current flows against the pressure gradient.

Several solutions were found for different values of $\nu_{\min}$. Surprisingly, when $\nu_{\min}$ was decreased to 1 cm^2/s, the maximum alongshore surface current *decreased* from 47 cm/s to 26 cm/s. The flow field was also more surface trapped. Similarly, when $\nu_{\min}$ was increased to 100 cm^2/s, the maximum alongshore surface current *increased* to 74 cm/s and the flow was less surface trapped. Only for values of $\nu_{\min}$ greater than 200 cm^2/s did the flow eventually begin to weaken, as might be expected.

The weakening of the coastal circulation as $\nu_{\min} \to 0$ is due to the β-effect. In an inviscid model, β allows the coastal circulation to leak offshore completely via the radiation of Rossby waves (Anderson and Gill, 1975). Vertical mixing inhibits this process, essentially by damping out the Rossby waves associated with higher-order baroclinic modes before they can propagate very far offshore (McCreary, 1981). The offshore leakage appears mathematically in the boundary solution (15) in that one of the roots of (16), k_1 say, vanishes as $\omega \to 0$. With $k_1 = 0$ it follows that $P_2 = 0$, and the boundary solution reduces to the negative of the interior solution (13).

Solutions vary with ν_h as expected. When ν_h was increaed to 10^6 cm^2/s, the maximum alongshore current decreased to 26 cm/s and occurred farther offshore at $x = -19$ km. When ν_h was decreased to 10^4 cm^2/sec, the current maximum increased to 71 cm/s at $x = -4$ km.

c. Periodic density-driven flow. In several oceans the surface buoyancy forcing is seasonal. Off the west coast of India, for example, a meridional surface density gradient appears in the Arabian Sea during the winter primarily due to salinity effects. It is therefore of interest to examine the effect of periodicity on buoyancy-forced flows.

Figure 8 shows a meridional section of the unbounded u' field when ρ_s oscillates at the annual cycle and $\nu_{\min} = 10$ cm^2/s. The phase is shown in months, with a negative number corresponding to a phase lag of u' with respect to the forcing. The amplitude of the current is weaker and more surface trapped than that of the comparable steady flow in Figure 4. There is downward phase propagation, and the surface current lags the forcing by about 1.5 months.

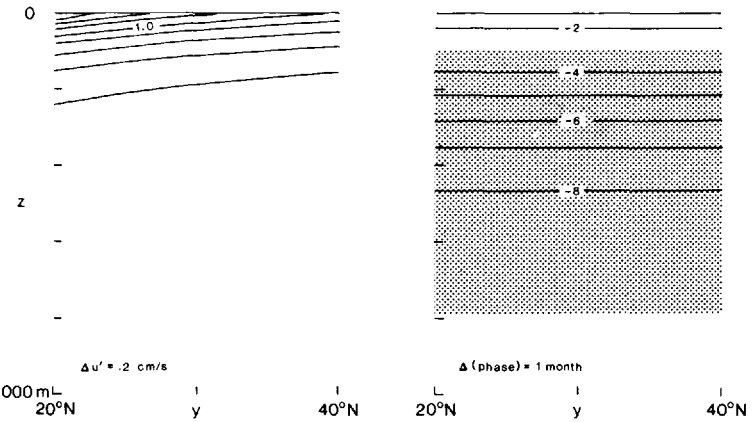

Figure 8. A meridional section showing u' when the surface density forcing ρ_s oscillates at the annual cycle. The amplitude and phase (in months) of u' are shown in the left and right panels, respectively. Negative phase indicates that u' lags ρ_s, and the value of the lag at the surface is 1.5 months. The region with lag values from -3 to -9 months is shaded. At $t = 0$, therefore, currents are eastward in unshaded regions and westward in shaded regions. The surface current is shallower and weaker than the corresponding steady flow in Figure 4. Phase propagates downward. It is this interior current that drives the coastal circulation in Figure 9.

The above properties occur because the effects of ρ_s are now confined to a diffusive surface boundary layer. To illustrate the important features of this layer, consider the solution of (14) when κ is constant. It immediately follows that $\rho' = \rho_s \exp(imz - i\sigma t)$ where $m = -(1 + i)(\sigma/2\kappa)^{1/2}$, a solution that has a boundary layer of thickness $(2\kappa/\sigma)^{1/2}$. The resulting expression for u', obtained directly from (1), is $u' = (g\rho_{sy}/f)(\kappa/\sigma)^{1/2} \exp(imz - i\sigma t + i\pi/4)$. The zonal velocity therefore lags the density forcing by $\pi/4$ radians (1.5 months at the annual cycle), a value very close to that in Figure 8.

Figure 9 is a meridional section at $x = -8$ km, showing the amplitude and phase of v near the coast. The response has a quasi-steady character in several ways. The amplitude and vertical structure of the currents are very similar to those of the steady solution in Figure 6; for example, at $t = 0$ the currents in regions where phase is unshaded are directed poleward, whereas those in shaded regions are equatorward. There is a relative minimum of the amplitude at a depth of about 200 m, and phase changes rapidly by several months across the minimum; this property indicates that the solution looks much like a vertically standing wave. The response is not quasi-steady in other ways. Phase lead increases with depth, so that phase propagates upward everywhere. Thus, part of the coastal response is well described as a vertically propagating wave that is carrying energy downward as well as poleward. Such a wave results from a superposition of Kelvin waves associated with several different baroclinic modes (Romea and Allen, 1983; see also McCreary, 1984, for a relevant discussion concerning vertically propagating, equatorial Kelvin waves).

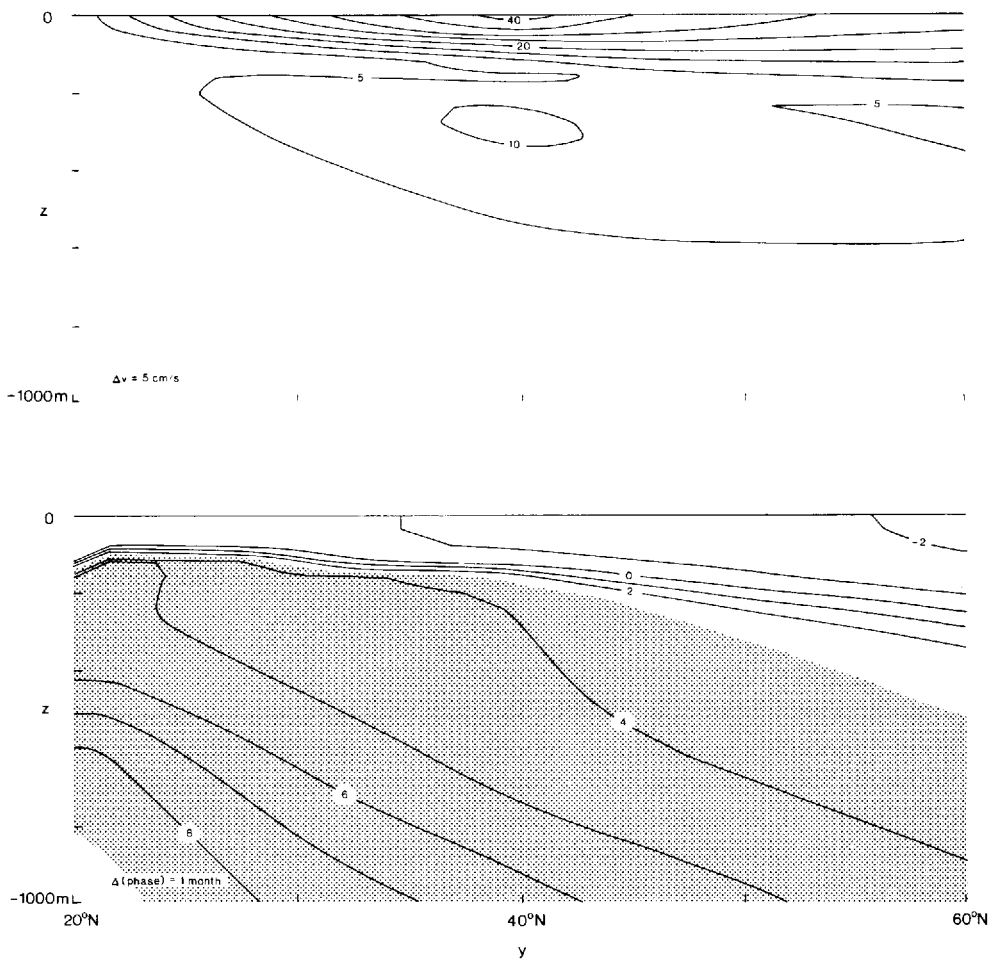

Figure 9. A meridional section at $x = -8$ km showing the amplitude and phase (in months) of v in the upper and lower panels, respectively, when the forcing ρ_s oscillates at the annual cycle. Positive phase indicates that v leads ρ_s. The shaded region indicates where the lead has values from 3 to 9 months. At $t = 0$, currents are poleward in unshaded regions and equatorward in shaded regions, and this vertical structure is very similar to the corresponding steady flow in Figure 6. There is a relative minimum in v across which phase changes rapidly, indicating that the solution has characteristics of a vertically standing wave. Phase propagates upward everywhere, however, indicating that it also looks like a vertically propagating Kelvin wave.

Unlike the case for steady forcing, the interior flow here does depend on ν_{min}. To investigate this dependence, we repeated the calculations of Figures 8 and 9 with $\nu_{min} = 1$ cm^2/s for the interior solution and $\nu_{min} = 10$ cm^2/s for the coastal response. As suggested by the above analysis, both the strength and the vertical scale of u' decreased by about a factor of 3 from that in Figure 8. As a result, the net transport of water

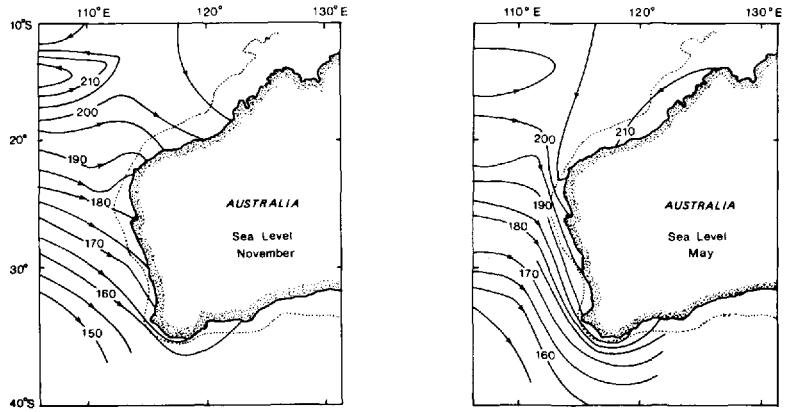

Figure 10. Observed dynamic height of the sea surface relative to 1300 db in November (left panel) and in May (right panel). There is a marked change in sea level topography near the coast, with pressure lines bending more sharply to the south in May. In contrast, the sea level gradient offshore is relatively unchanged throughout the year. The wind field near the coast is strongly seasonal, being strongest (most equatorward) in the southern-hemisphere summer (November) and essentially vanishing in winter (May). (After Godfrey and Ridgway, 1985.)

toward the eastern boundary decreased by an order of magnitude and the alongshore current weakened by a similar amount.

d. Application to the Leeuwin Current. As noted in the Introduction the Leeuwin Current off Australia has a prominent seasonal cycle. Figure 10 contrasts the observed surface dynamic height field in November when the current is near its minimum strength (left panel) with that in May when it attains its maximum (right panel). This variability cannot be related to offshore variations in sea level; note in Figure 10 that the sea-surface slope 1000 km offshore is practically constant throughout the year. Rather it appears to be wind-driven since the opposing wind is almost absent in the southern-hemisphere winter (May) and reaches a maximum strength in the summer. The observations suggest, then, that the coastal circulation off Australia is significantly forced by a steady sea-surface density field ρ_s and a seasonally varying wind stress τ^y.

The solution presented in this section is driven by an idealized forcing chosen to resemble that off the west coast of Australia. The model is again forced by the steady thermohaline forcing (22), although this forcing may somewhat underestimate the actual buoyancy driving off Australia. In addition, a seasonal wind stress is introduced in the form

$$\tau^y = -\tau_0 Y(y)(1 + \cos \sigma t), \tag{24}$$

where $\tau_0 = 0.5$ dyn/cm^2 and $\sigma = 2\pi$/year. The meridional profile of the wind $Y(y)$ increases linearly from zero at 22.5N to maximum strength from 25N to 30N and then

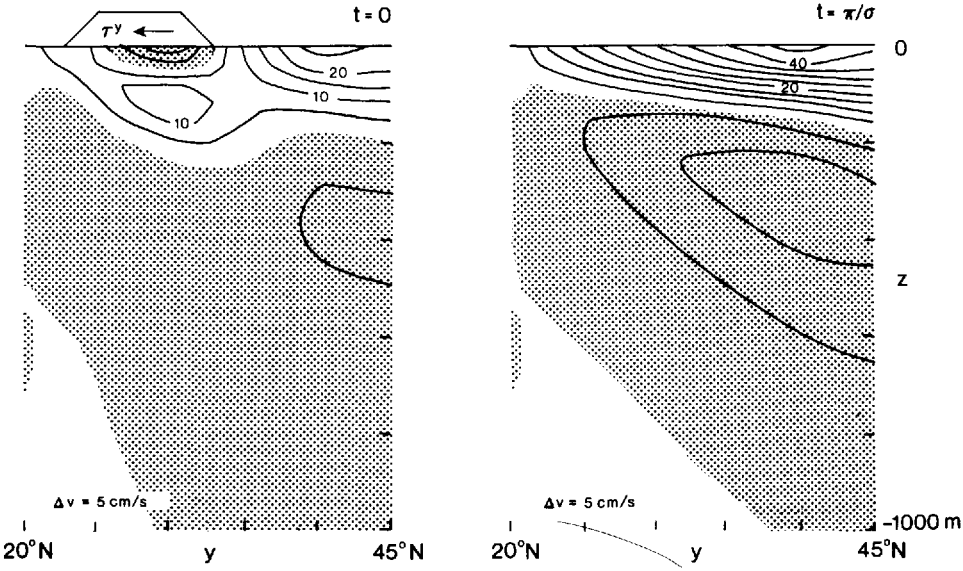

Figure 11. Meridional sections at $x = -8$ km showing v when the model is forced by a steady surface density forcing (22) and a seasonally varying equatorward wind (24). The left panel shows the response at $t = 0$ when the winds are strongest, whereas the right panel shows the response at $t = \pi/\sigma$ when they are weakest. The meridional profile of the wind is indicated in the figure. The coastal circulation is weakened, and even reversed, by the wind.

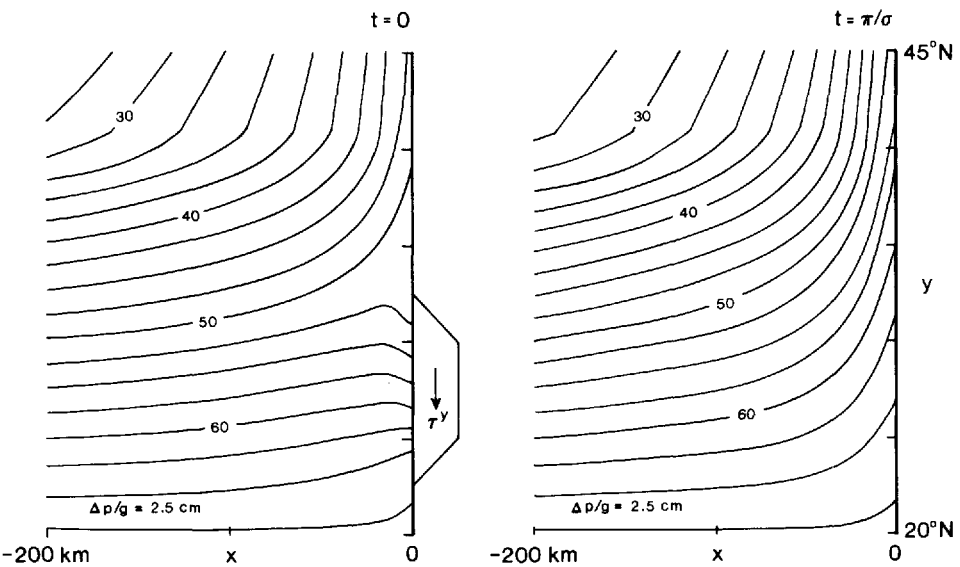

Figure 12. As in Figure 11, except showing horizontal sections of sea level. The poleward drop in sea level at the coast is intensified by the wind. Compare this figure to the observed annual response off Australia in Figure 10.

decreases linearly to zero at 32.5N; it is indicated in Figures 11 and 12. The wind is put into the ocean as a body force G with $h = 50$ m.

Figure 11 shows the resulting alongshore flow field at $t = 0$ (left panel) when the equatorward wind is 1 dyn/cm^2, and at $t = \pi/\sigma$ (right panel) when the wind is zero. At $t = 0$ the model response from 25N to 30N is typical for upwelling regions, albeit weak; the surface flow is equatorward and there is a poleward undercurrent. Off Australia the surface flow at the corresponding time is weak but still poleward; this behavior can be simulated in the model by assuming a somewhat larger buoyancy driving or a weaker wind. The distribution of the currents at $t = \pi/\sigma$, when $\tau^y = 0$, is essentially that due to steady buoyancy driving alone (Fig. 6).

Figure 12 shows the surface pressure field at the two instants. The poleward flow is strongest when the poleward sea-surface gradient *at the coast* is weakest, namely at $t = \pi/\sigma$. The strong equatorward wind at $t = 0$ increases the opposing coastal sea level slope in the latitude band of the wind. This pattern of seasonal change is qualitatively similar to the observed one in Figure 10. Coastal tide gauge data allow a more quantitative comparison. The sea level drop from Carnarvon (25S) to Freemantle (32S) is 14 cm in January when the winds are strong, but only 4 cm in July when they are weak (see Fig. 4 and 5 of Godfrey and Ridgway, 1985).

Figure 13 shows the phase of the variable part of the surface pressure field, the part driven only by τ^y. Phase propagates both offshore and poleward. Poleward propagation speeds decrease offshore, varying from a value of 75 cm/s at $x = -50$ km to 15 cm/s at $x = -200$ km. Godfrey and Ridgway (1985; their Fig. 4) noted a similar propagation of the seasonal component of the observed surface dynamic height. They remarked that the observed poleward propagation speed of 30 cm/s was much smaller than that of any low-order mode internal Kelvin wave, but provided no explanation for this phenomenon. Recall from section 2c that Rossby waves associated with the $n = 1$ and 2 baroclinic modes exist poleward of 20N. The variability evident in Figure 13 is due to the offshore radiation of these waves. Because the wavelength of the Rossby waves decreases with latitude ($k_{1y} > 0$ in the northern hemisphere), their westward phase speed decreases poleward. Consequently, phase lines bend offshore at lower latitudes, and there is an apparent poleward phase propagation associated with their radiation offshore.

The above solution differs from the observations in several ways. First, the model undercurrent is weaker than the surface current, whereas the observed one is comparable in strength (Fig. 2). This difference is likely due to the unrealistic increase of ν with depth required by the specification (2). Second, the annual-mean speed of the model Leeuwin Current is too small, reaching a maximum value of only 37 cm/s at 40N compared to the observed annual mean of over 50 cm/s. One explanation for this difference is that the values for the mixing coefficients are not correct; it is possible, for example, to increase the maximum mean speed to 53 cm/s by reducing ν_h to 10^4 cm^2/s. Another possibility is that the remote forcing mechanism mentioned in the Introduction also contributes to the Leeuwin Current. Finally, Godfrey (private communica-

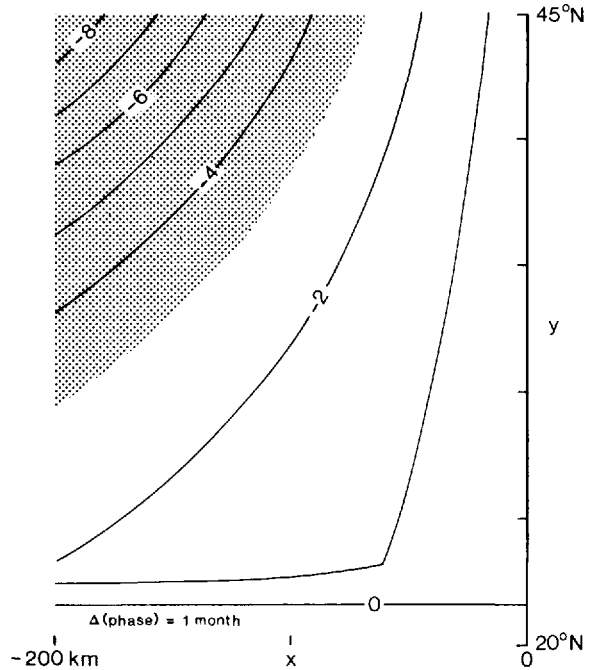

Figure 13. As in Figure 12, except showing the phase of the annually varying part of the sea level signal. Negative phase indicates that sea level lags τ^y. The region with lag values less than -3 months is shaded. Phase propagates both offshore and poleward due to the radiation of Rossby waves from the coast.

tion) has pointed out that the seasonal change in the alongshore gradient of the dynamic height field somewhat offshore (near the shelf break) is in the opposite sense to that of the tide gauges, with the maximum gradient occurring in May when the winds are weak (see Figure 11 of Godfrey and Ridgway, 1985). This property cannot be simulated by our model, and again suggests the possible importance of remote forcing.

4. Summary and discussion

This paper investigates the response of the eastern ocean to thermohaline forcing by a specified, longitudinally independent surface density field ρ_s. The model ocean is a generalization of the wind-driven model of McCreary (1981) to include forcing by ρ_s. Solutions are expressed as the sum of a forced interior solution and a coastal response, and each piece can be associated with a different value of ν. Solutions are shown for both steady and annually varying forcings.

When ρ_s is steady, the density field in the interior ocean is affected throughout the water column and is independent of the magnitude of κ. Provided that ρ_s increases poleward, a poleward pressure gradient field and an associated eastward geostrophic

current are established in the upper ocean (Fig. 4). This current forces downwelling at an eastern ocean boundary, and generates a poleward surface current and an equatorward undercurrent there (Figs. 5 and 6). Sea level slopes downward toward the pole everywhere, the slope being weakest at the coast (Fig. 7). The dynamic height field at the depth of the undercurrent is much flatter, but slopes upward toward the pole; it has a dome around which there is cyclonic flow. The importance of vertical mixing in the dynamics of the steady coastal circulation is evident in that all currents vanish as $\nu \rightarrow 0$. This property is due to the β-effect; without vertical mixing the westward propagation of Rossby waves allows the coastal currents to leak completely offshore. Solutions depend on ν_h in the expected manner, with currents becoming weaker and broader as ν_h increases.

When ρ_s oscillates at the annual cycle, the density field in the interior ocean is affected only in a boundary layer of thickness $(2\kappa/\sigma)^{1/2}$. The resulting pressure gradient field and the geostrophic zonal currents are correspondingly surface trapped (Fig. 8). Phase propagates *downward* through this flow field, and the interior surface current lags the forcing by 1.5 months. The coastal currents generated by this forcing are qualitatively quasi-steady; at $t = 0$ they have an amplitude and vertical structure similar to those of the steady solution (Fig. 9). Phase propagates *upward* everywhere, however, indicating that part of the coastal response is a vertically-propagating Kelvin wave carrying energy downward.

The driving of the coastal circulation off the west coast of Australia is modelled by a steady thermohaline forcing ρ_s and a seasonally varying equatorward wind τ^y, and the model response compares well with observations of currents and dynamic height fields. Compare, for example, Figure 1 with Figure 7 and Figure 10 with Figure 12. In particular, there is a model Leeuwin Current that attains its maximum strength in the southern-hemisphere winter when the opposing winds are weakest (Fig. 11). In addition, both model and observations exhibit offshore and poleward phase propagation of the annual component of the surface dynamic height field (Fig. 13). In the model this variability is due to the offshore propagation of Rossby waves generated by τ^y at the coast. Some aspects of the response do not agree with the observations, and these differences indicate that remote forcing may also contribute to the Leeuwin Current.

The successful comparison summarized in the previous paragraph suggests that a significant part of the coastal circulation off Australia is driven by thermohaline forcing. Is this forcing mechanism important elsewhere? There are other examples of surface coastal currents that flow against the wind. The poleward Davidson Current develops off the coast of California when the equatorward winds relax in the late fall and winter (Sverdrup *et al.*, 1942; Hickey; 1979; Chelton, 1984). Similarly, a poleward countercurrent appears off the west coast of India during the winter, when the winds weaken considerably and there is a poleward density gradient in the Arabian Sea (Shetye, 1984). It may be that thermohaline forcing is responsible for generating these and other currents as well.

Acknowledgments. This work was supported by ONR Grant No. N00014-85-K-0019 and by NSF Grant No. OCE-8509752. The Department of Science and Technology, Government of India, and the National Science Foundation provided funds for Satish Shetye to visit the Joint Institute of Marine and Atmospheric Research at the University of Hawaii, thereby making our collaboration possible. Computations were performed on the CRAY-1 computer at the National Center for Atmospheric Research, which is supported by the National Science Foundation. We would like to thank Stuart Godfrey, who first brought to our attention the remarkable characteristics of the Leeuwin Current; his comments and suggestions were invaluable. We also thank Kevin Kohler for his programming assistance and Kathy Maxson for drafting the figures.

REFERENCES

Anderson, D. L. T. and A. E. Gill. 1975. Spin-up of a stratified ocean, with applications to upwelling. Deep-Sea Res., *22,* 583–596.

Chelton, D. B. 1984. Seasonal variability of alongshore geostrophic velocity off central California. J. Geophys. Res., *89(C3),* 3473–3486.

Godfrey, J. S. and K. R. Ridgway. 1985. The large scale environment of the poleward flowing Leeuwin current, western Australia: Longshore steric height gradients, wind stresses and geostrophic flow. J. Phys. Oceanogr., *15,* 481–495.

Hickey, B. M. 1979. The California current system—hypotheses and facts. Prog. Oceanogr., *8,* 191–279.

McCreary, J. P. 1980. Modelling wind-driven ocean circulation. Tech. Rep. HIG-80-3, Hawaii Inst. Geophys., Honolulu, HI, 64 pp.

McCreary, J. P. 1981. A linear stratified ocean model of the coastal undercurrent. Phil. Trans. Roy. Soc. Lond. *A302,* 385–413.

McCreary, J. P. 1984. Equatorial beams. J. Mar. Res., *42,* 395–430.

McCreary, J. P. and P. K. Kundu. 1985. Western boundary circulation driven by an alongshore wind: With application to the Somali Current system. J. Mar. Res., *43,* 493–516.

Moore, D. W. 1968. Planetary-gravity waves in an equatorial ocean. Ph.D. thesis, Harvard University, Cambridge, MA.

Pacanowski, R. C. and S. G. H. Philander. 1981. Parameterization of vertical mixing in numerical models of tropical oceans. J. Phys Oceanogr., *11,* 1443–1451.

Romea, R. D. and J. S. Allen. 1983. On vertically propagating coastal Kelvin waves at low latitudes. J. Phys. Oceanogr., *13,* 1241–1254.

Rothstein, L. M. 1984. A model of the equatorial sea surface temperature field and associated circulation dynamics. J. Phys. Oceanogr., *14,* 1875–1892.

Shetye, S. R. 1984. Seasonal variability of the temperature field off the south-west coast of India. Proc. Indian Acad. Sci. (Earth Planet. Sci.), *93,* 399–411.

Stommel, H. 1965. The Gulf Stream, Univ. California Press, 248 pp.

Sverdrup, H. U., M. W. Johnson and R. H. Fleming. 1942. The Oceans, Prentice-Hall, 1087 pp.

Thompson, R. O. R. Y. 1984. Observations of the Leeuwin Current off western Australia. J. Phys. Oceanogr., *14,* 623–628.

Received: *12 July, 1985;* revised: *20 November, 1985.*